Applied Physics Letters ARTICLE scitation.org/journal/apl

Modeling the electrical degradation of AlGaN-based UV-C LEDs by combined deep-level optical spectroscopy and TCAD simulations

Cite as: Appl. Phys. Lett. **122**, 161105 (2023); doi: 10.1063/5.0144721
Submitted: 31 January 2023 · Accepted: 7 April 2023 ·
Published Online: 20 April 2023

View Online Export Citation CrossMark

Nicola Roccato,[1,a)] Francesco Piva,[1] Carlo De Santi,[1] Matteo Buffolo,[1] Manuel Fregolent,[1] Marco Pilati,[1] Norman Susilo,[2] Daniel Hauer Vidal,[2] Anton Muhin,[2] Luca Sulmoni,[2] Tim Wernicke,[2] Michael Kneissl,[2,3] Gaudenzio Meneghesso,[1] Enrico Zanoni,[1] and Matteo Meneghini[1,4]

AFFILIATIONS

[1]Department of Information Engineering, University of Padova, via Gradenigo 6/B, Padova 35131, Italy
[2]Technische Universität Berlin, Institute of Solid State Physics, Hardenberstr. 36, Berlin 10623, Germany
[3]Ferdidnand-Braun-Institut (FBH), Gustav-Kirchhoff-Str.. 4, Berlin 12489, Germany
[4]Department of Physics and Astronomy, University of Padova, via Marzolo 8, Padova 35131, Italy

Note: This paper is part of the APL Special Collection on UV/DUV Light Emitters.
[a)]**Author to whom correspondence should be addressed:** roccatonic@dei.unipd.it

ABSTRACT

The long-term stability of ultraviolet (UV)-C light-emitting diodes (LEDs) is of major importance for many applications. To improve the understanding in this field, we analyzed the degradation of AlGaN-based UVC LEDs and modeled the variation of electrical characteristics by 2D simulations based on the results of deep-level optical spectroscopy (DLOS). The increase in the forward leakage current observed during ageing was ascribed an increase in trap-assisted tunneling. The analysis of the degradation kinetics suggests the role of a defect diffusion process, possibly involving impurities coming from the p-type layers.

Ultraviolet (UV) light-emitting diodes (LEDs) are ideal candidates to replace conventional mercury gas-discharge lamps in several applications such as disinfection, curing, gas sensing, and skin safe disinfection,[1–6] thanks to their smaller size, lower energy consumption, fast switching, and emission wavelength.[7] However, for most applications, UV LEDs (especially in the UV-C range) may still have a short lifetime.[8,9] In recent years, numerous investigations have been carried out on the reliability of AlGaN-based UV LEDs,[10–16] but the physical mechanisms responsible for degradation of these devices have not been completely understood; among the issues that still remain under investigation are the increase in the drive voltage during ageing,[14] the generation of mid-gap states in the active region,[15] and the migration of impurities.[16]

In this paper, 265 nm UV LEDs submitted to constant-current stress at 100 A cm^{-2} are analyzed. We propose a model that accurately reproduces the electrical degradation of these devices. The measured increase in the forward leakage current during ageing is attributed to an increase in trap-assisted tunneling (TAT), related to the generation/propagation of defect states within, and close to the active region. Technology computer aided design (TCAD) simulations were carried out to support this hypothesis based on defect properties obtained through deep-level optical spectroscopy (DLOS) analysis. The results allowed us to accurately reproduce the experimental data and suggest the presence of a diffusion process responsible for the increase in defect states near the active region. The modeling approach described in this paper represents a useful methodology for a first-order quantitative assessment of the local defect density exhibiting mid-gap states and their evolution as a consequence of ageing within the device.

The analyzed LEDs were grown on an AlN-sapphire substrate by metalorganic vapor phase epitaxy (MOVPE). The epitaxial structure is grown on high temperature annealed (HTA) epitaxially laterally overgrown (ELO) AlN on sapphire with a threading dislocation density of 9×10^{8} cm^{-2}.[17] The LED heterostructure growth on HTA-ELO AlN/sapphire starts with a 400 nm AlN layer, followed by a 25 nm AlGaN

Si-doped layer. Then a 1 μm Si-doped $Al_{0.76}Ga_{0.24}N$ buffer layer and a 100 nm $Al_{0.65}Ga_{0.35}N$ Si-doped transition layer are grown, followed by a 200 nm Si-doped $Al_{0.65}Ga_{0.35}N$ contact layer with $N_D = 4 \times 10^{18}$ cm^{-3}. A single 1.4 nm $Al_{0.48}Ga_{0.52}N$ quantum well (QW) is then placed between a 38 nm thick Si-doped $Al_{0.62}Ga_{0.38}N$ lower barrier and a 10 nm $Al_{0.62}Ga_{0.38}N$ undoped upper barrier. An undoped 10 nm $Al_{0.8}Ga_{0.2}N$ interlayer, separating the p-region from the last barrier, was included to reduce the LED turn on voltage.[7] Above this layer, a 25 nm p-doped $Al_{0.75}Ga_{0.25}N$ layer works as an electron blocking layer (EBL) with a nominal Mg concentration of 1×10^{19} cm^{-3} and is followed by a p-doped 230 nm GaN layer with a Mg concentration of 6×10^{19} cm^{-3}. The LEDs were fabricated by standard micro-fabrication techniques using Pd/Au p-contacts and V/Al based n-contacts.[18] The nominal emission wavelength is 265 nm, and the area is 1×10^{-3} cm^2. The devices investigated here resemble previously studied devices[8,17] but exhibit a single quantum well, thus allowing for a simpler interpretation of DLOS data and TCAD.

The devices were operated at a constant current stress at 100 A/cm^2 (100 mA) for more than 300 h (19 000 min) at a heat sink temperature of 25 °C. During the constant current stress, the electrical characteristics were monitored through current–voltage (I–V) measurements at logarithmic time intervals. Figure 1 reports the variation of the electrical characteristics during stress. Significant forward and reverse leakage currents are observed and increased during ageing time. During stress, we observed a slight shift of the turn-on voltage and an increase in the series resistance (voltage > 5.5 V), which we attribute to a degradation of the contact at the p-side[19] or to the formation of potential barriers reducing carrier injection efficiency.[20]

Recent papers indicated that in the low forward bias region, conduction is mainly dominated by trap-assisted tunneling (TAT).[21–23] This mechanism strongly depends on the density of defects in the depleted region. Thus, the observed increase in the forward leakage current suggests an increase in defect concentration induced by the stress experiment,[24] which are characterized by DLOS and their effect on the low bias leakage current simulated subsequently. Additionally, we observe an increased leakage current in the reverse bias direction, indicating a reduction of the shunt resistance of the device.[25]

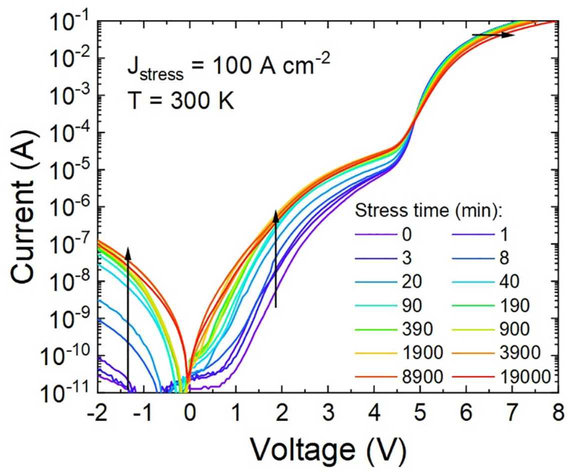

FIG. 1. I–V characteristic of the device during constant current stress at 100 A/cm^2 in the semilogarithmic scale.

In order to characterize the anticipated deep levels generated during the stress test and likely located in proximity to the active region of the device, we performed DLOS analysis. As explained in Ref. 26, the measurement consists in monitoring the transient device capacitance under monochromatic illumination and is sensitive to the photoinduced charging or discharging of defect states in the depletion region. From the analysis of the steady-state photocapacitance transients, information on trap density and ionization energy can be obtained.

The analysis was performed at 0 V, i.e., the space charge region reached the $Al_{0.62}Ga_{0.38}N$:Si first barrier from the end of the $Al_{0.75}Ga_{0.25}N$ EBL, including an at least 25 nm wide region. The results allow one to extract the concentration of defects responding to a given photon energy [Fig. 2(a)]. We observe an increasing generation of optically excited charges for photon energies > 2.2 eV peaking at 2×10^{16} cm^{-3} for 3.4 eV. We note here that the measurements done at energies higher than 3.4 eV are partly affected by significant absorption/generation in the p-GaN layer, and this causes a reduction in the ΔC leading to a reduction in N_T as shown in Fig. 2(a).

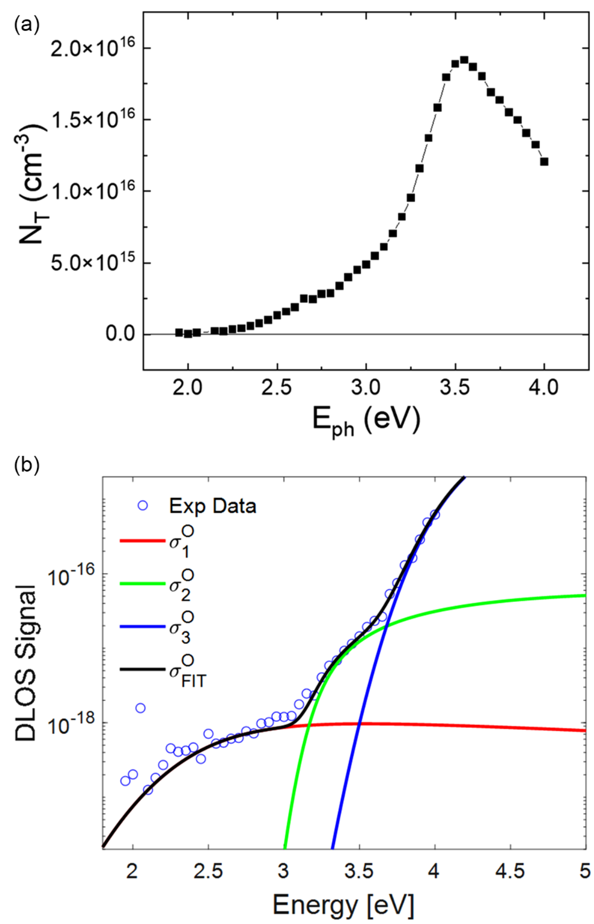

FIG. 2. (a) Measurement of the density of traps responding to a specific photon energy. (b) DLOS signal obtained as a function of the photon energy. Circles are the experimental data; red, green, and blue lines are the fits with the Pässler model for the three components identified; in black the sum of the three components.

The optical ionization energy of defects was then evaluated through photoionization cross section analysis.[27] First, we extracted the DLOS signal, as the inverse of the product between the time constant of the photo-capacitance transient and the photon flux ϕ [Fig. 2(b)].

The experimental data are then fitted using the model proposed by Pässler *et al.*,[26,27]

$$\sigma(h\nu, T) \simeq \frac{const.}{h\nu\sqrt{2\pi d_{FC}\epsilon \coth\left(\frac{\epsilon}{2k_B T}\right)}} \times \int_0^{(+\infty)} dE_k \frac{E_k^{\frac{3}{2}}}{(E_k + E^O - d_{FC})^2} \times \exp\left[-\frac{(h\nu - E^O - E_k)^2}{2d_{FC}\epsilon \coth\left(\frac{\epsilon}{2k_B T}\right)}\right].$$

The model considers the lattice relaxation of the deep levels having given optical ionization energy (E^O) and Franck–Condon shift (d_{FC}). Here, k_B is the Boltzmann constant, T is the temperature, $\epsilon = h\nu$ is the effective phonon energy, and $E_k = h\nu - E_T$ is the kinetic energy of the excited electrons. The thermal ionization energy E_T (also referred to as the electron binding energy) can be calculated from the optical ionization energy as $E_T = E^O - d_{FC}$. As reported in Table I and in Fig. 2, three different deep levels have been identified at $E_{T,1} = E_C - 0.94$ eV, $E_{T,2} = E_C - 3.06$ eV, and $E_{T,3} = E_C - 3.52$ eV. The identified deep level energies are comparable with the ones found by Arehart and Armstrong.[28,29]

In order to model the electrical characteristic of the device, we employed the TCAD Sentaurus suite from Synopsys, Inc.[30,31] The layers were doped by placing the donor or acceptor traps (Si and Mg). The silicon was located at $E_C - 24$ meV for n-doped AlGaN layers, whereas magnesium was placed at $E_V + 150$ meV and $E_V + 380$ meV, respectively for the p-GaN layer and the $Al_{0.75}Ga_{0.25}N$ EBL.[32–34] We also set the typical parameters of radiative and Auger–Meitner mechanisms at 2×10^{-10} cm^3/s and 1×10^{-30} cm^6/s, respectively, according with the literature.[35–37]

In Fig. 3(a), we report the simulated band diagram at a forward bias of 2 V, along with the electron and hole concentrations; the respective layers are noted on the top x-axis. We can observe that at 2 V the QW is already full of electrons, and electrons accumulate at the interface between the interlayer and the last barrier (d = 285 nm), whereas the sharp interface between the p-GaN and the EBL favors the accumulation of holes (d = 250 nm) due to the strong bad discontinuity between the GaN and $Al_{0.75}Ga_{0.25}N$ layers. These detected accumulation regions are extremely important for our TAT modeling, since they represent preferential starting points for the tunneling process. To be more specific, TAT was implemented by the procedure described by Roccato *et al.*[24,38] and by Mandurrino *et al.*[39] We identified the most likely TAT path from the interlayer/last barrier interface (electron starting point) toward the undoped interlayer for electrons. For holes, three different starting points have been collocated in the EBL with a maximum of 10 nm of tunneling toward the interlayer. Only the traps present in the interlayer can contribute to TAT due to its position in the space charge region, its short distance to hole and electron containing layers, and the band bending, which allows a favorable alignment (in energy) between the carriers and the traps.[24,39,40] The implementation of TAT in this region is obtained through the addition of an additional SRH-like recombination process, whose capture rates define the tunneling probability[31,39,41,42] and whose main parameters have been chosen according to the literature.[39,42–44]

TABLE I. Values of E^0 and d_{FC} obtained from the fits of the three identified deep levels. The thermal ionization energy was calculated as $E_T = E^O - d_{FC}$.

	E^0 (eV)	d_{FC} (eV)	E_T (eV)
$E_{T,1}$	2.22	1.28	0.94
$E_{T,2}$	3.16	0.1	3.06
$E_{T,3}$	3.99	0.47	3.52

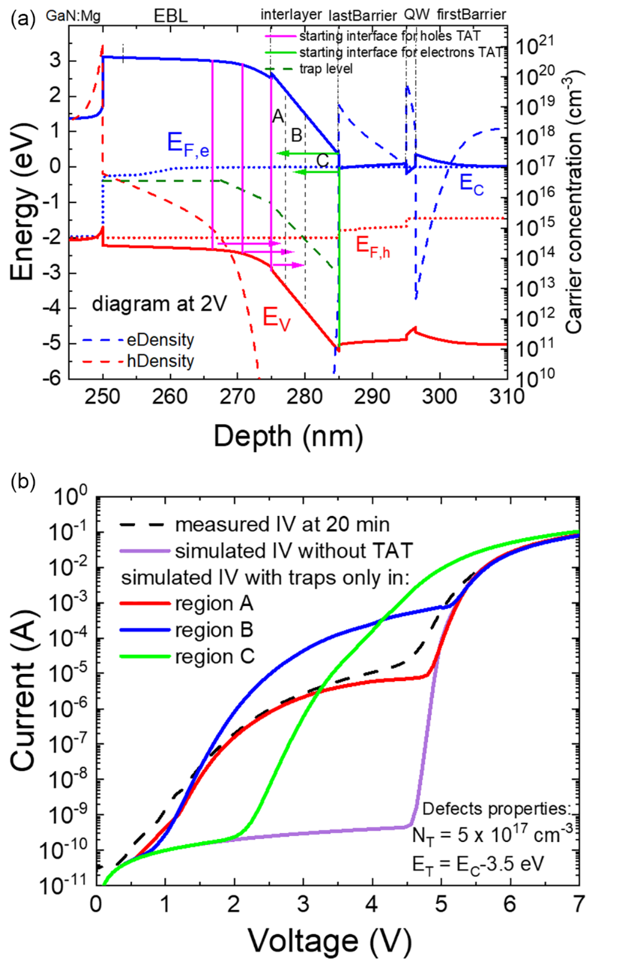

FIG. 3. (a) Simulated band diagram and carrier concentration of the device at 2 V. (b) Analysis of the contribution to TAT of the traps located in different regions of the undoped interlayer in comparison with the measured I–V curve after 20 min of operation.

For our simulations, a single trap level was placed near the midgap at the energy identified by DLOS analysis at E_C−3.5 eV with a Gaussian distribution in energy of $\sigma = 200$ meV in order to consider a realistic energy dispersion of the defect.[45,46] Only this level, in fact, contributes the most at low voltages to the TAT process due to its proximity to $E_{F,H}$.[24,39] Simulations performed with the shallower levels did not yield a significant TAT current.

To study how the spatial distribution of traps in the interlayer contributes to TAT, we divided this layer in three regions: region A is adjacent to the EBL (2 nm wide), region B is in the middle (3 nm wide), and region C (5 nm) is closer to the last barrier [Fig. 3(a)]. Initially, we keep an identical trap concentration in the three regions ($N_T = 5 \times 10^{17}\,\text{cm}^{-3}$ at the energy level of $E_T = 3.5\,eV$) and simulated the I–V characteristic by separately considering the effect of the traps located in each region. In Fig. 3(b), the analysis for the I–V curve measured after an operation time of 20 min is shown. (The same analysis was also performed for all other operation times.) To match the measured I–V curves, we also introduced a shunt resistance ($R_{SH} = 4 \times 10^{10}\,\Omega$) to consider parasitic current paths at low biases, a series resistance ($R_S = 14\,\Omega$) of the contacts, current spreading layers, etc.[47]

The comparison of the simulated I–V curves and the measured I–V curves shows that:

- Traps present in region C (closest to the n-side) contribute to a strong decrease in the turn-on voltage (green line). This effect is not observed on the real device (dashed).
- Traps located in region B contribute to the increase in the leakage current in the voltage range between 1 and 4 V, but such an increase is excessive (blue line). At reduced trap concentration, we observed an improved fit for voltages >2.5 V but a way too low current for V < 2.5 V.
- Traps located in region A (closer to the p-side) favor an increase in the leakage current at lower voltage compatible with the experimental values (red line). A relatively high defect concentration near the EBL is also expected from the literature due to its the proximity with a layer featuring a high p-doping.[16]

Once we understood how the three regions contribute to TAT, the trap density in each section was used as fitting parameter to match the experimental I–V curves obtained from the constant current stress. For the data in Fig. 3(b), a trap concentration of 5×10^{17} cm^{-3} in region A, 1×10^{16} cm^{-3} in region B, and 2×10^{15} cm^{-3} in region C yield the best fit.

Figure 4 shows a comparison between the measured and simulated electrical characteristics during the stress. To provide a correct match, we changed only trap concentrations and the series resistances according to values reported in Table II. It is worth noticing that: (i) the good correspondence obtained at low voltages between simulated and experimental curves is in the TAT-assisted conduction region. Results, thus, confirm the contribution of the deep levels to forward leakage current. (ii) The estimated trap concentrations exhibit a monotonically increasing trend within the interlayer, which is compatible with the generation/diffusion of defects occurring during the constant current stress.[48] (iii) The parallel shunt resistance determined from the reverse leakage current in the range between 0 and −1 V (see also Fig. 1) increases with stress time and for >20 min has a significant contribution to the forward leakage current until 2 V.[25] Finally, (iv) the extrapolated trap concentrations decrease from region A, adjacent to the EBL, toward region C, closer to the last barrier. In addition, we observe a strong increase in the defect density in the first region, compared to the other two regions. This behavior can be explained by either a localized generation of defects or, more probably, a diffusion process originating from the p-region and directed toward the active region.[16]

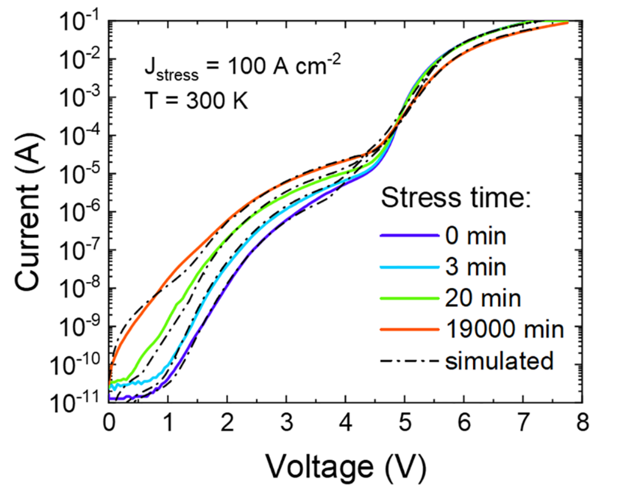

FIG. 4. Simulated I–V curves during ageing mainly modeled by an increase in the trap concentration in the interlayer.

To test the hypothesis of a diffusion process, we compared the modeled increase in the trap concentration with an ideal diffusion process originating from the EBL and directed toward the interlayer region. We employ the diffusion model proposed by Orita *et al.*[49] and assume a sufficiently large and constant concentration of the diffusing impurity N_0 at the interface between EBL and interlayer. Under these assumptions, the time-dependent concentration of the diffusing impurity at a position z follows the equation:

$$N_{diff}(z) = N_0 erfc\left(\frac{z}{2\sqrt{Dt}}\right), \tag{1}$$

where D is the coefficient of diffusion, t is the stress time, and z is the distance from the EBL/interlayer interface. Therefore, the relation between the average trap concentration in a region of interest and the stress time can be expressed as

TABLE II. Estimated trap concentration, series and shunt resistances used as fitting parameters for the TCAD-assisted modeling of the I–V curves measured during stress. The trap concentrations are referred to the midgap deep level at $E_C - 3.5$ eV subdivided in their spatial region.

Time (min)	$N_{T,A}$ (cm^{-3})	$N_{T,B}$(cm^{-3})	$N_{T,C}$(cm^{-3})	R_S (Ω)	R_P (Ω)
0	2×10^{16}	3×10^{15}	1×10^{15}	14	4×10^{10}
3	1.3×10^{17}	5×10^{15}	1×10^{15}	14	3×10^{10}
20	5×10^{17}	1×10^{16}	2×10^{15}	14	1×10^{10}
19 000	1.5×10^{18}	2×10^{16}	7×10^{15}	18	5×10^{8}

$$N_T = \frac{N_0}{w}\int_0^w erfc\left(\frac{z}{2\sqrt{Dt}}\right)dz, \quad (2)$$

where w is the width of the region of interest. In our case, we considered as a reference region the one with the greatest defect concentration, i.e., region A, which is 2 nm wide.

Figure 5 reports the simulated defect concentration data obtained through this approach by using N_0 and D as fitting parameters. Remarkably, the diffusion model can effectively reproduce the experimental data, suggesting that a migration of impurities is effectively taking place. The most significative parameter extrapolated from the fit is the diffusion coefficient D, whose extrapolated value was found to be $2.1\ \times 10^{-18}\ cm^2\ s^{-1}$. We note that this is a realistic value, already reported in the literature for the diffusion of hydrogen in gallium nitride.[49,50] Also Glaab *et al.*[16] found, by SIMS measurements, that the concentration of hydrogen atoms (above $1 \times 10^{17}\ cm^{-3}$) similar to the fitted N_0 is present in the p-type material due to incorporation during growth, even after thermal annealing. Hydrogen typically occurs as interstitials bound to Mg acceptors[51] or with negatively charged point defects, such as group-III vacancies,[40] forming defect complexes. The authors also found that H migrates toward the n-side during the stress.[16] Here, it is important to note that the diffusion has to be initiated by exciting the hydrogen atoms from the complex. Knauer *et al.* identified high energy holes from Auger-processes triggering the degradation.[52] These could give the energy necessary for the assumed diffusion process. However, further work is necessary to clearly identify the point defects and their interaction with hydrogen[19] and if the same defects are responsible for the increase in nonradiative recombination and lower injection efficiency. The method presented here is a key technique to determine the point defect density and its evolution during ageing in the junctions and should be further exploited to determine the degradation processes.

We analyzed the electrical degradation of SQW AlGaN-based UV-C LEDs by a constant current stress carried out at $100\ A/cm^2$. The experimental investigation, aided by DLOS measurements, allowed us to identify three distinct deep levels at $E_C - 0.94$ eV, $E_C - 3.06$ eV, and $E_C - 3.52$ eV. The increase in the leakage current induced by constant current stress could be ascribed to an increase in the trap-assisted tunneling components. The I–V measurements collected during stress were accurately reproduced by assuming a monotonic increase in the density of the deep level traps within the interlayer volume close to the EBL. The degradation kinetics was found to be consistent with a defect migration process, and a model was proposed and adopted. From a global standpoint, we can conclude that: (i) trap assisted tunneling is the main mechanism that contributes to the forward sub-threshold leakage current in UV-C LEDs, and (ii) this process is strongly determined by the concentration of the deeper levels located closer to the EBL. Additionally, we demonstrated that (iii) it is possible to build a model that emulates the forward leakage current variation of the electrical behavior of the device during ageing by employing the trap concentration in a specific device layer as the fitting parameter.

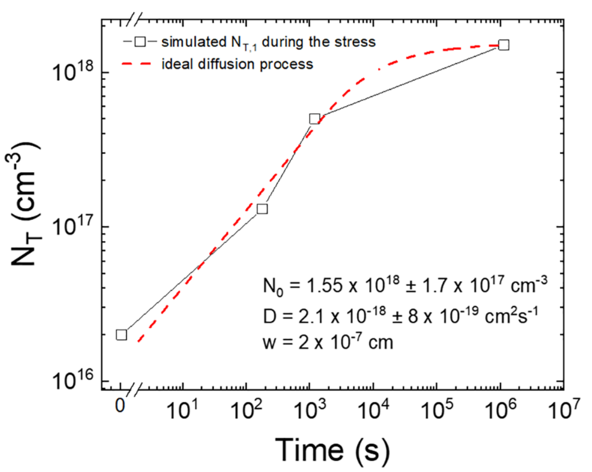

FIG. 5. Comparison between the trap concentration estimated by simulations in region A adjacent to the EBL during the stress and the *impurity profile described by* an ideal diffusion process *originating* from the EBL.

The authors thank Sylvia Hagedorn (FBH) and Sebastian Walde (FBH) for providing ELO AlN/sapphire substrates and Praphat Sonka for operating and maintaining the MOVPE-system. This work was partially supported by the Federal Ministry of Education and Research (BMBF) through the Twenty20 initiative "Advanced UV for Life."

AUTHOR DECLARATIONS

Conflict of Interest

The authors have no conflicts to disclose.

Author Contributions

Nicola Roccato: Conceptualization (equal); Data curation (equal); Formal analysis (lead); Investigation (equal); Methodology (lead); Software (lead); Visualization (equal); Writing – original draft (lead); Writing – review & editing (lead). **Luca Sulmoni:** Resources (equal); Visualization (supporting). **Tim Wernicke:** Funding acquisition (supporting); Investigation (supporting); Project administration (supporting); Resources (equal); Supervision (supporting); Visualization (equal); Writing – original draft (supporting). **Michael Kneissl:** Funding acquisition (supporting); Investigation (supporting); Resources (equal); Supervision (supporting); Visualization (supporting); Writing – original draft (supporting). **Gaudenzio Meneghesso:** Funding acquisition (equal); Resources (equal). **Enrico Zanoni:** Funding acquisition (equal); Resources (equal). **Matteo Meneghini:** Funding acquisition (equal); Investigation (supporting); Methodology (supporting); Project administration (lead); Supervision (lead); Visualization (equal); Writing – original draft (supporting). **Francesco Piva:** Conceptualization (equal); Data curation (equal); Formal analysis (equal); Investigation (equal); Visualization (equal); Writing – original draft (supporting). **Carlo De Santi:** Conceptualization (equal); Data curation (supporting); Formal analysis (equal); Investigation (equal); Methodology (equal); Visualization (equal). **Matteo Buffolo:** Conceptualization (equal); Data curation (equal); Formal analysis (equal); Methodology (supporting); Writing – original draft (supporting). **Manuel Fregolent:** Data curation (supporting). **Marco Pilati:** Data curation (supporting); Investigation (supporting). **Norman Susilo:** Resources (equal). **Daniel Hauer Vidal:** Resources (equal). **Anton Muhin:** Resources (equal); Visualization (supporting).

DATA AVAILABILITY

The data that support the findings of this study are available from the corresponding author upon reasonable request.

REFERENCES

[1]W. S. Won, L. G. Tran, W. T. Park, K. K. Kim, C. S. Shin, N. Kim, Y. J. Kim, and Y. J. Yoon, "UV-LEDs for the disinfection and bio-sensing applications," Int. J. Precis. Eng. Manuf. **19**, 1901–1915 (2018).
[2]C. Dreyer and F. Mildner, "Application of LEDs for UV-curing," Mater. Sci. **227**, 415–434 (2016).
[3]M. Schreiner, J. Mar Tí Nez-Abaigar, J. Glaab, and M. Jansen, "UV-B induced secondary plant metabolites," Opt. Photonik **9**, 34–37 (2014).
[4]J. Glaab, N. Lobo-Ploch, H. K. Cho, T. Filler, H. Gundlach, M. Guttmann, S. Hagedorn, S. B. Lohan, F. Mehnke, J. Schleusener, C. Sicher, L. Sulmoni, T. Wernicke, L. Wittenbecher, U. Woggon, P. Zwicker, A. Kramer, M. C. Meinke, M. Kneissl, M. Weyers, U. Winterwerber, and S. Einfeldt, "Skin tolerant inactivation of multiresistant pathogens using far-UVC LEDs," Sci. Rep. **11**, 14647 (2021).
[5]M. A. Würtele, T. Kolbe, M. Lipsz, A. Külberg, M. Weyers, M. Kneissl, and M. Jekel, "Application of GaN-based ultraviolet-C light emitting diodes–UV LEDs–for water disinfection," Water Res. **45**, 1481–1489 (2011).
[6]K. Michael and J. Rass, *III-Nitride Ultraviolet Emitters* (Springer International Publishing, Cham, 2016).
[7]H. Amano, R. Collazo, C. De Santi, S. Einfeldt, M. Funato, J. Glaab, S. Hagedorn, A. Hirano, H. Hirayama, R. Ishii, Y. Kashima, Y. Kawakami, R. Kirste, M. Kneissl, R. Martin, F. Mehnke, M. Meneghini, A. Ougazzaden, P. J. Parbrook, S. Rajan, P. Reddy, F. Römer, J. Ruschel, B. Sarkar, F. Scholz, L. J. Schowalter, P. Shields, Z. Sitar, L. Sulmoni, T. Wang, T. Wernicke, M. Weyers, B. Witzigmann, Y.-R. Wu, T. Wunderer, and Y. Zhang, "The 2020 UV emitter roadmap," J. Phys. D Appl. Phys. **53**, 503001 (2020).
[8]J. Ruschel, J. Glaab, N. Susilo, S. Hagedorn, S. Walde, E. Ziffer, H. K. Cho, N. L. Ploch, T. Wernicke, M. Weyers, S. Einfeldt, and M. Kneissl, "Reliability of UVC LEDs fabricated on AlN/sapphire templates with different threading dislocation densities," Appl. Phys. Lett. **117**, 241104 (2020).
[9]J. Glaab, J. Ruschel, N. Lobo Ploch, H. K. Cho, F. Mehnke, L. Sulmoni, M. Guttmann, T. Wernicke, M. Weyers, S. Einfeldt, and M. Kneissl, "Impact of operation parameters on the degradation of 233 nm AlGaN-based far-UVC LEDs," J. Appl. Phys. **131**, 014501 (2022).
[10]H. Hirayama, S. Fujikawa, and N. Kamata, "Recent progress in AlGaN-based deep-UV LEDs," Electron. Commun. Jpn. **98**, 1–8 (2015).
[11]N. Trivellin, D. Fiorimonte, F. Piva, M. Buffolo, C. De Santi, G. Meneghesso, E. Zanoni, and M. Meneghini, "Reliability of commercial UVC LEDs: 2022 state-of-the-art," Electronics **11**, 728 (2022).
[12]M. A. Khan, "AlGaN multiple quantum well based deep UV LEDs and their applications," Phys. Status Solidi **203**, 1764–1770 (2006).
[13]F. Piva, C. De Santi, M. Deki, M. Kushimoto, H. Amano, H. Tomozawa, N. Shibata, G. Meneghesso, E. Zanoni, and M. Meneghini, "Stability and degradation of AlGaN-based UV-B LEDs: Role of doping and semiconductor defects," Microelectron. Reliab. **100–101**, 113418 (2019).
[14]J. Rass, J. Ruschel, J. Glaab, I. Ostermay, and S. Einfeldt, "Impact of insulators and their deposition method on the reliability of AlInGaN-based UVB LEDs," IEEE Photonics Technol. Lett. **32**, 1007–1010 (2020).
[15]J. Glaab, J. Haefke, J. Ruschel, M. Brendel, J. Rass, T. Kolbe, A. Knauer, M. Weyers, S. Einfeldt, M. Guttmann, C. Kuhn, J. Enslin, T. Wernicke, and M. Kneissl, "Degradation effects of the active region in UV-C light-emitting diodes," J. Appl. Phys. **123**, 104502 (2018).
[16]J. Glaab, J. Ruschel, T. Kolbe, A. Knauer, J. Rass, H. K. Cho, N. Lobo Ploch, S. Kreutzmann, S. Einfeldt, M. Weyers, and M. Kneissl, "Degradation of (In)AlGaN-Based UVB LEDs and migration of hydrogen," IEEE Photonics Technol. Lett. **31**, 529–532 (2019).
[17]N. Susilo, E. Ziffer, S. Hagedorn, L. Cancellara, C. Netzel, N. Lobo Ploch, S. Wu, J. Rass, S. Walde, L. Sulmoni, M. Guttmann, T. Wernicke, M. Albrecht, M. Weyers, and M. Kneissl, "Improved performance UVC-LEDs by combination high-temperature annealing epitaxially laterally overgrown AlN/sapphire," Photonics Res. **8**, 589 (2020).
[18]L. Sulmoni, F. Mehnke, A. Mogilatenko, A. Mogilatenko, M. Guttmann, T. Wernicke, M. Kneissl, and M. Kneissl, "Electrical properties and microstructure formation of V/Al-based n-contacts on high Al mole fraction n-AlGaN layers," Photonics Res. **8**(8), 1381–1387 (2020).
[19]M. Meneghini, D. Barbisan, Y. Bilenko, M. Shatalov, J. Yang, R. Gaska, G. Meneghesso, and E. Zanoni, "Defect-related degradation of deep-UV-LEDs," Microelectron. Reliab. **50**, 1538–1542 (2010).
[20]C. De Santi, E. Zanoni, F. Piva, G. Meneghesso, H. Amano, H. Tomozawa, M. Deki, M. Kushimoto, M. Meneghini, and N. Shibata, "Modeling the degradation mechanisms of AlGaN-based UV-C LEDs: From injection efficiency to mid-gap state generation," Photonics Res. **8**(11), 1786–1791 (2020).
[21]C. De Santi, M. Buffolo, N. Renso, A. Neviani, G. Meneghesso, E. Zanoni, and M. Meneghini, "Evidence for defect-assisted tunneling and recombination at extremely low current in InGaN/GaN-based LEDs," Appl. Phys. Express **12**, 052007 (2019).
[22]N. Renso, C. De Santi, A. Caria, F. Dalla Torre, L. Zecchin, G. Meneghesso, E. Zanoni, and M. Meneghini, "Degradation of InGaN-based LEDs: Demonstration of a recombination-dependent defect-generation process," J. Appl. Phys. **127**, 185701 (2020).
[23]M. Auf Der Maur, B. Galler, I. Pietzonka, M. Strassburg, H. Lugauer, and A. Di Carlo, "Trap-assisted tunneling in InGaN/GaN single-quantum-well light-emitting diodes," Appl. Phys. Lett. **105**, 133504 (2014).
[24]N. Roccato, F. Piva, C. de Santi, R. Brescancin, K. Mukherjee, M. Buffolo, C. Haller, J.-F. Carlin, N. Grandjean, M. Vallone, A. Tibaldi, F. Bertazzi, M. Goano, G. Verzellesi, G. Meneghesso, E. Zanoni, and M. Meneghini, "Modeling the electrical characteristics of InGaN/GaN LED structures based on experimentally-measured defect characteristics," J. Phys. D. Appl. Phys. **54**, 425105 (2021).
[25]E. Jung, J. K. Lee, M. S. Kim, and H. Kim, "Leakage current analysis of GaN-based light-emitting diodes using a parasitic diode model," IEEE Trans. Electron Devices **62**, 3322–3325 (2015).
[26]M. Buffolo, A. Caria, F. Piva, N. Roccato, C. Casu, C. De Santi, N. Trivellin, G. Meneghesso, E. Zanoni, and M. Meneghini, "Defects and reliability of GaN-based LEDs: Review and perspectives," Phys. Status Solidi **219**, 2100727 (2022).
[27]R. Pässler, "Photoionization cross-section analysis for a deep trap contributing to current collapse in GaN field-effect transistors," J. Appl. Phys. **96**, 715–722 (2004).
[28]B. R. Aaron Arehart, P. A. Steven Ringel, A. Leonard Brillson, and S. Rajan, "Investigation of electrically active defects in GaN, AlGaN, and AlGaN/GaN high electron mobility transistors," Ph.D. thesis (Ohio State University, 2009), pp. 163.
[29]A. Armstrong, A. Chakraborty, J. S. Speck, S. P. DenBaars, U. K. Mishra, and S. A. Ringel, "Quantitative observation and discrimination of AlGaN- and GaN-related deep levels in AlGaN/GaN heterostructures using capacitance deep level optical spectroscopy," Appl. Phys. Lett. **89**, 262116 (2006).
[30]Synopsys, Inc., "Sentaurus^{TM} device user guide," 2015, see http://www.synopsys.com/Company/Pages/Trademarks.aspx (accessed on August 2, 2020).
[31]Synopsys, Inc., "Sentaurus^{TM} structure editor user guide destination control statement," 2015, see http://www.synopsys.com/Company/Pages/Trademarks.aspx (accessed on July 30, 2020).
[32]C. Z. Zhao, T. Wei, L. Y. Chen, S. S. Wang, and J. Wang, "The activation energy for Mg acceptor in AlxGa1-xN alloys in the whole composition range," Superlattices Microstruct. **109**, 758–762 (2017).
[33]Y. Nakano and T. Jimbo, "Electrical properties of acceptor levels in Mg-doped GaN," Phys. Status Solidi. **0**(1), 438–442 (2003).
[34]L. Silvestri, K. Dunn, S. Prawer, and F. Ladouceur, "Hybrid functional study of Si and O donors in wurtzite AlN," Appl. Phys. Lett. **99**, 122109 (2011).
[35]R. Ni, Z. Yu, Z. Liu, L. Zhang, L. Jia, and Y. Zhang, "Light extraction and auger recombination in AlGaN-based ultraviolet light-emitting diodes," IEEE Photonics Technol. Lett. **32**, 971–974 (2020).
[36]F. Nippert, M. Tollabi Mazraehno, M. J. Davies, M. P. Hoffmann, H. J. Lugauer, T. Kure, M. Kneissl, A. Hoffmann, and M. R. Wagner, "Auger recombination in AlGaN quantum wells for UV light-emitting diodes," Appl. Phys. Lett. **113**, 071107 (2018).
[37]P. Pampili and P. J. Parbrook, "Doping of III-nitride materials," Mater. Sci. Semicond. Process **62**, 180–191 (2017).

[38]N. Roccato, F. Piva, C. De Santi, M. Buffolo, C. Haller, J.-F. Carlin, N. Grandjean, M. Vallone, A. Tibaldi, F. Bertazzi, M. Goano, G. Verzellesi, G. Meneghesso, E. Zanoni, and M. Meneghini, "Modeling the electrical characteristic of InGaN/GaN blue-violet LED structure under electrical stress," Microelectron. Reliab. **138**, 114724 (2022).

[39]M. Mandurrino, G. Verzellesi, M. Goano, M. Vallone, F. Bertazzi, G. Ghione, M. Meneghini, G. Meneghesso, and E. Zanoni, "Physics-based modeling and experimental implications of trap-assisted tunneling in InGaN/GaN light-emitting diodes," Phys. Status Solidi **212**, 947–953 (2015).

[40]C. G. van de Walle and J. Neugebauer, "First-principles calculations for defects and impurities: Applications to III-nitrides," J. Appl. Phys. **95**, 3851 (2004).

[41]F. Jiménez-Molinos, F. Gámiz, A. Palma, P. Cartujo, and J. A. López-Villanueva, "Direct and trap-assisted elastic tunneling through ultrathin gate oxides," J. Appl. Phys. **91**, 5116–5124 (2002).

[42]M. Mandurrino, M. Goano, M. Vallone, F. Bertazzi, G. Ghione, G. Verzellesi, M. Meneghini, G. Meneghesso, and E. Zanoni, "Semiclassical simulation of trap-assisted tunneling in GaN-based light-emitting diodes," J. Comput. Electron. **14**, 444–455 (2015).

[43]M. Levinshtein, S. L. Rumyantsev, and M. S. Shur, *Properties of Advanced Semiconductor Materials: GaN, AIN, InN, BN, SiC, SiGe* (Wiley, 2001).

[44]A. Alkauskas, M. D. McCluskey, and C. G. van de Walle, "Tutorial: Defects in semiconductors—Combining experiment and theory," J. Appl. Phys. **119**, 181101 (2016).

[45]N. Modolo, C. de Santi, G. Baratella, A. Bettini, M. Borga, N. Posthuma, B. Bakeroot, S. You, S. Decoutere, A. Bevilacqua, A. Neviani, G. Meneghesso, E. Zanoni, and M. Meneghini, "Compact modeling of nonideal trapping/detrapping processes in GaN power devices," IEEE Trans. Electron Devices **69**, 4432–4437 (2022).

[46]B. Srocka, H. Schener, and D. Bimberg, "Fe +-Fe + level as a recombination center in Ino 53Gao 47As," Phys. Rev. B **49**, 10259 (1994).

[47]N. S. Averkiev, A. E. Chernyakov, M. E. Levinshtein, P. V. Petrov, E. B. Yakimov, N. M. Shmidt, and E. I. Shabunina, "Two channels of non-radiative recombination in InGaN/GaN LEDs," Phys. B Condens. Matter **404**, 4896–4898 (2009).

[48]Z. Ma, H. Cao, S. Lin, X. Li, and L. Zhao, "Degradation and failure mechanism of AlGaN-based UVC-LEDs," Solid. State. Electron **156**, 92–96 (2019).

[49]K. Orita, M. Meneghini, H. Ohno, N. Trivellin, N. Ikedo, S. Takigawa, M. Yuri, T. Tanaka, E. Zanoni, and G. Meneghesso, "Analysis of diffusion-related gradual degradation of InGaN-based laser diodes," IEEE J. Quantum Electron. **48**, 1169–1176 (2012).

[50]C. de Santi, M. Meneghini, G. Meneghesso, and E. Zanoni, "Degradation of InGaN laser diodes caused by temperature- and current-driven diffusion processes," Microelectron. Reliab. **64**, 623–626 (2016).

[51]S. Nakamura, N. Iwasa, M. Senoh, and T. Mukai, "Hole compensation mechanism of p-type GaN films," Jpn. J. Appl. Phys. **31**, 1258–1266 (1992).

[52]A. Knauer, T. Kolbe, S. Einfeldt, J. Glaab, B. Beidoun, N. L. Ploch, M. Weyers, J. Ruschel, J. Rass, and M. Kneissl, "Current-induced degradation and lifetime prediction of 310 nm ultraviolet light-emitting diodes," Photonics Res. **7**(7), B36–B40 (2019).